

SOLID FREEFORM FABRICATION

Electrospinning 3D Nanofiber Structure of Polycaprolactone Incorporated with Silver Nanoparticles

YINGGE ZHOU,¹ MAHESH THAKURATHI,² EDWARD L. QUITEVIS,² and GEORGE Z. TAN^{1,3}

1.—Department of Industrial, Manufacturing, and Systems Engineering, Texas Tech University, Lubbock, TX, USA. 2.—Department of Chemistry and Biochemistry, Texas Tech University, Lubbock, TX, USA. 3.—e-mail: george.z.tan@ttu.edu

This study presents a one-station 3D fabrication technique of nanofibrous scaffold for tissue engineering. A divergence static electric field was introduced in an electrospinning system to induce a self-assembly of aligned polycaprolactone (PCL) nanofibers into a tunable 3D architecture with thickness ranging from 2 to 12 mm. Silver nanoparticles were incorporated into the PCL solution to alter the electrical conductivity. Human fibroblast cells were cultured on the pure PCL nanofiber scaffolds *in vitro* for 7 days. It was found that the occurrence of nanofiber bridging phenomenon depended on the solution viscosity. The minimum viscosity to form a 3D nanofiber structure was higher than that to form a 2D nanofiber mat. The homogeneity of nanofiber distribution within the 3D space was positively correlated with the electrical conductivity and the weight of the nanofibers. In the cell culture test, fibroblasts proliferated on the scaffold and organized as an aligned matrix which mimicked the microstructure of native musculoskeletal tissues.

INTRODUCTION

The demand for human organ substitutes and the limited availability of transplant donors has advanced the development of tissue engineering. Usually, tissue engineering involves the use of artificial scaffolds to provide architectural cues for cell growth.¹ Generally, there are two categories of scaffold fabrication processes: top-down or bottom-up methods.² In top-down approaches, the cells are seeded in the scaffolds before the formation of biological resemble geometries. With bottom-up approaches, cells and biomaterials are integrated in modular units that form composite architecture. Common top-down approaches include solvent casting, particulate-leaching techniques, gas foaming, phase separation, freeze drying, melt molding, electrospinning and others. Latest strategies focus on creating a biomimetic cell topology of extracellular matrix (ECM) that closely simulate gradient architecture in natural tissues. ECM is a three-dimensional (3D) structure that regulates cellular function and maintains tissue architecture.³ ECM components such as heparin and heparan sulfate bind growth factors and slowly release them to cells,

to obtain sustainable release.⁴ It was found that microscale and nanoscale topography of ECM effects cell behavior by providing biochemical and biophysical stimuli to promote cell adhesion, proliferation, morphogenesis, and motility.^{5,6} For example, ECM signaling can regulate pancreas branching morphogenesis by controlling collective cellular dynamics.⁷ There are several critical physical features of ECM to consider when fabricating biomimetic scaffolds, including its dimensionality, porosity, architecture, stiffness, ligand topography, and density.⁸

Despite rapid progress in engineering relatively simple tissues, there is a research need in integrating the tunable microarchitecture in heterogeneous scaffolds to closely resemble natural tissue structures. Electrospinning is a versatile technique which has been widely applied in scaffold fabrication and modification in tissue engineering. The processing flexibility of electrospinning enables fiber fabrication from various materials, ranging from synthetic polymers,⁹ natural polymers to mixed polymers embedded with functional additives,¹⁰ such as collagen, gelatin, elastin, silk, poly(L-lactic acid), poly(glycolic acid), poly

(ϵ -caprolactone) (PCL) and poly(lactic-co-glycolic) acid.¹¹ PCL is one of the most commonly used biomaterials for scaffolds due to its crystalline nature which gives it a slow degradation rate and suitable mechanical properties. Electrospinning has shown a promising capability of creating scaffolds with a random or aligned fibrous microstructure.^{12–14} In addition, efforts have been made to construct 3D electrospun structures, including vertical stacking layers of fiber membranes,¹⁵ incorporating nanofibers with hydrogel,¹⁶ rolling the nanofiber mat into a cylinder,¹⁷ particle leaching,¹⁸ and combining nanofibers with 3D printing,¹⁹ etc. These strategies require additional procedures or complex configurations which may lead to a higher risk in quality control, lower production efficiency and increased overall cost. Therefore, one of the key research needs is to fabricate biomimetic scaffolds with intrinsic structural properties by a high-efficiency technique with minimized procedures.

In this paper, we present a rapid fabrication technique of a 3D nanofibrous scaffold for tissue engineering. A divergence static electric field was introduced in an electrospinning system to induce a self-assembly of aligned PCL nanofibers into a 3D architecture.²⁰ We hypothesized that: (1) the formation of a 3D nanofiber structure depends on the viscosity of the polymer solution; and (2) the nanofiber distribution along the z -axis can be affected by the electrical conductivity of the polymer solution. The objective of this study is to investigate the effects of viscosity and conductivity of polymer solution on nanofiber diameter and density within the 3D fibrous scaffold. A cell culture test was performed to demonstrate the feasibility of providing 3D physical cues to guide cell growth by the nanofiber scaffold.

MATERIALS AND METHODS

Polymer Solution Preparation

PCL polymer solutions were prepared by dissolving 5 wt.%, 6 wt.%, 7 wt.%, 10 wt.%, and 15 wt.% PCL pellets (MW = 80,000; Sigma-Aldrich®, St. Louis, MO, USA) in an organic solvent. The solvent was prepared by homogenizing N,N -Dimethylformamide (99.8%; Sigma-Aldrich®) and acetone (Thermo Fisher Scientific, Waltham, MA, USA) at a volume ratio of 1:1. The solution was magnetically stirred for 4 h at room temperature until there were no visible suspended particulates. To adjust the electrical conductivity of the polymer solution, silver nanoparticles (AgNP; 40–50 nm; MTI, Richmond, CA, USA) were added into the PCL solution. The composite solution was homogenized by 20 kHz sonication for 30 s (Q125 Sonicator; Qsonica, Newtown, CT, USA).

Electrospinning Configuration

The divergence electrospinning was configured based on a high-voltage direct-current power source

and a specially-designed polylactic acid (PLA) collector. The design of the collector is demonstrated in Fig. 1a. The collector was comprised of two tilted surfaces, which had an inclination angle of 45° to the collector bottom. The width of collector was 40 mm and the height was 20 mm. This double-bevel collector was 3D printed by the Ultimaker3 system (Ultimaker®, The Netherlands). Aluminum foil was glued on the inner surface of each bevel using PCL solution, and was connected to the aluminum wire through a small central hole on the bevel.

The collector was placed on an insulating stand in the electrospinning chamber. The aluminum foils on the collectors were grounded separately using electrical wires passing through the inner cavity of the stand (Fig. 1b). The PCL solution syringe was set to be 10 cm above the bottom center of the collector, and was pumped with a rate of 1 mL/h. The voltage was set to be 10 kV, and the electrospinning time was approximately 2 min. The double-bevel induced a divergent electric field so that nanofibers were deposited onto both bevels of the collector while forming connecting fibers inbetween.

Polymer Solution Characterization

The viscosity of PCL solution was measured by a Fungilab ALPHA series digital rotational viscometer (Fungilab, New York, NY, USA) at 23°C with three rotation speeds: 50 rpm, 60 rpm, and 100 rpm. The viscosity was recorded every 20 s. Conductivity of the solutions was measured using a Cole-Parmer benchtop pH/conductivity meter (Cole-Parmer Instruments; Vernon Hills, IL, USA). The electrode was immersed in the solution and the measurement was carried out at room temperature (23°C), and the equipment was calibrated with standard calibration solutions of known conductivity.

Scaffold Characterization

To characterize the internal nanofiber distribution, the nanofibers within the scaffold were collected by moving a customized glass slide perpendicular to the fiber alignment direction. The nanofiber morphology was examined by scanning electron microscopy (SEM; Phenom ProX; NanoScience, Alexandria, VA, USA). Fiber diameter was analyzed by ImageJ. A total of 20 fibers were measured for each sample. Fiber density was characterized by counting the number of fibers that intersected a line (length = 54 μ m) drawn across the middle of a binary SEM images under $\times 5000$ magnification. Top, middle, and bottom sections were selected for fiber density analysis. Energy-dispersive x-ray spectroscopy (EDS) was performed to confirm the presence of AgNPs in the electrospun nanofibers.

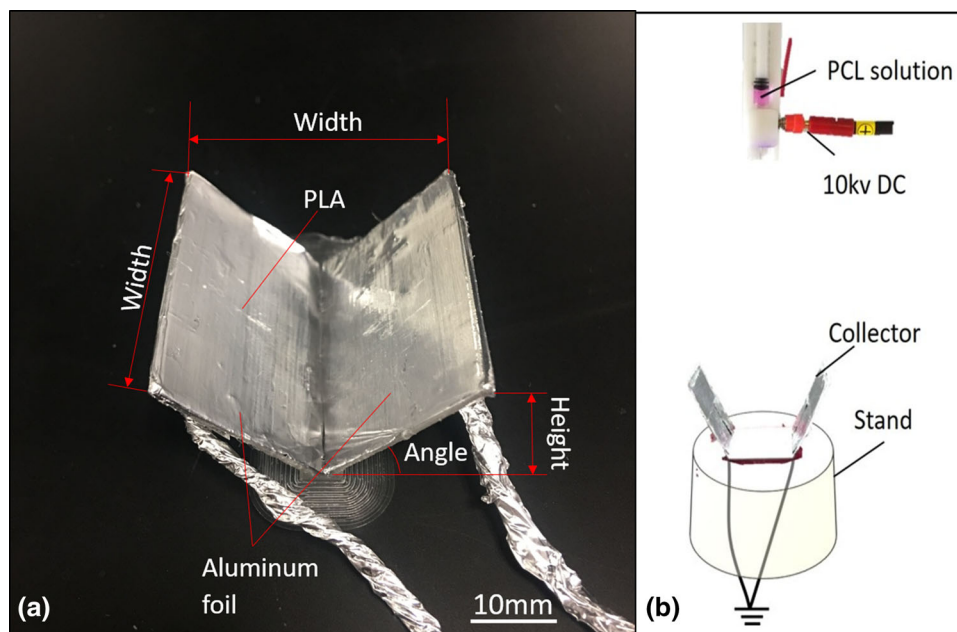


Fig. 1. (a) Collector design. (b) Divergence electrospinning configuration.

Cell Culture

We fabricated a scaled-down scaffold (20 mm × 10 mm, width × length) to fit the tissue culture plate. The collector was immersed in 70% ethanol for 30 min prior to electrospinning. The electrospinning chamber was sprayed and wiped with 70% ethanol and maintained sterile during the electrospinning process. After the nanofiber scaffold was obtained, the collector and the scaffold were sterilized by UV light in the biosafety cabinet for 30 min. The scaffold in the collector was then placed in a sterile 50-ml beaker. Human fibroblast cells (ATCC[®], MRC-5) were suspended in complete growth medium. The medium was slowly added into the beaker to cover the scaffold. The cell-seeded microfiber was incubated for 7 days. Cells were fixed with 4% formaldehyde after 7 days. For microscope imaging, cells were stained with CruzFluor Phalloidin fluorescence conjugate and 4',6-diamidino-2-phenylindole (DAPI) for cell cytoplasm and nucleus, respectively.

RESULTS

The viscosities of PCL solutions are shown in Fig. 2a. All solutions were Newtonian fluids. When the PCL concentration was below 7%, we did not observe a formation of 3D nanofibers between the two bevels. Instead, only 2D fiber mats were deposited on the inner surfaces of the two bevels. When the PCL concentration reached 7% (viscosity reached 207.8 mPa s), the divergent electric field induced a nanofiber deposition on the surfaces of both bevels, meanwhile the whipping process led to a self-assembly of nanofiber between the two bevels

(Fig. 2b). Furthermore, the fiber bundle with highly aligned fibers were formed from bottom to top and the fiber density increased from bottom to top. Addition of AgNPs slightly increased the viscosity of the solution. The mean viscosity of 15% PCL was 2418.2 mPa s, those of AgNP incorporated PCL were 2706.7 mPa s (0.1% AgNP), 2754 mPa s (0.5% AgNP), and 2853.8 mPa s (1% AgNP).

Interestingly, the addition of AgNPs decreased the electrical conductivity of the PCL solution (Fig. 3a). The solutions were cast and observed under the SEM. The AgNPs agglomerated into sub-micro particles which were uniformly distributed in the PCL solution (Fig. 3b–d). There was no trend in particle agglomeration as the AgNP concentration increased. Although silver is conductive, it is not surprising that all the solutions were non-conductive because of the scarcity of ion carriers in the organic solvents (DMF and chloroform). The molar conductivity, which is obtained by dividing the ionic conductivity by the electrolyte concentration, is inversely proportional to viscosity.²¹ We speculate that AgNPs bound to the PCL and reduced its mobility, thus reduced the conductivity of the solution. The exact mechanisms of conductivity decrease need to be explored in future studies.

Representative SEM images of electrospun nanofibers are shown in Fig. 4. The fibers were highly aligned and AgNPs were embedded in the nanofibers. The EDS confirmed the presence of silver (Fig. 5). A summary of nanofiber diameters is presented in Fig. 6a. The fiber diameter was positively correlated to the solution viscosity. The 10% PCL resulted in a mean diameter of 296.4 nm while the 15% PCL resulted in a mean diameter of 359.6 nm. By adding 0.1% and 0.5% AgNPs, the

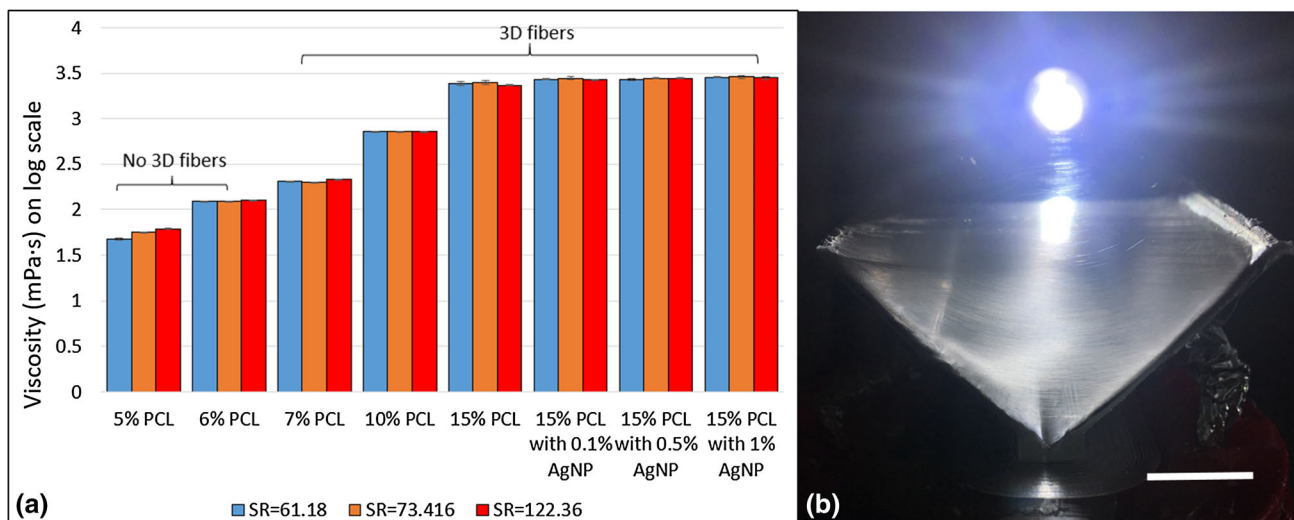


Fig. 2. (a) A summary of PCL solution viscosities. *SR* shear rate (S^{-1}), (b) a 3D nanofiber scaffold fabricated by divergence electrospinning. Scale bar 1 cm.

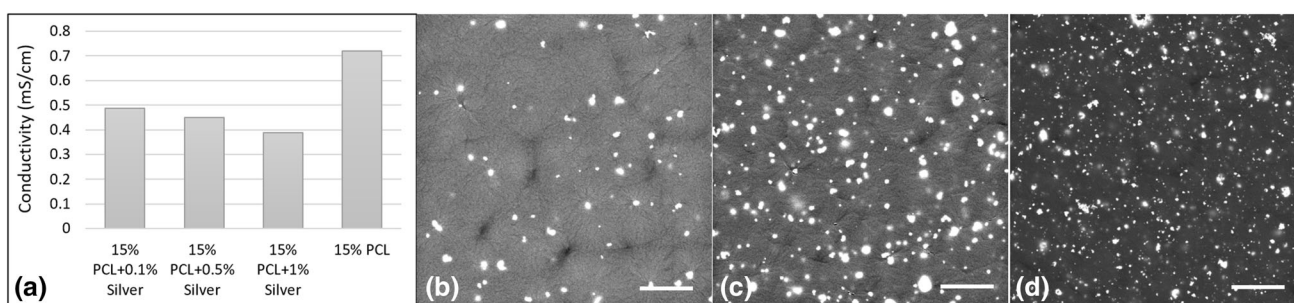


Fig. 3. (a) Electrical conductivities of PCL solution with and without AgNPs. SEM images of solidified PCL solutions with AgNP: (b) 15% PCL with 0.1% AgNP; (c) 15% PCL with 0.5% AgNP; (d) 15% PCL with 1% AgNP. Scale bar 10 μm.

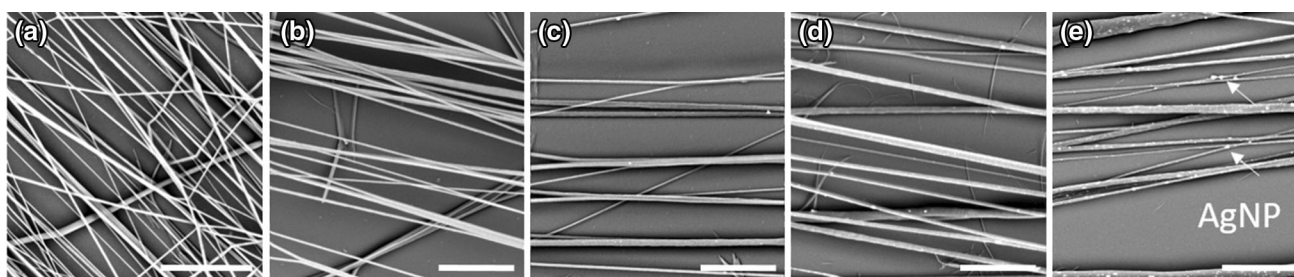


Fig. 4. SEM images of electrospun nanofibers: (a) 10% PCL; (b) 15% PCL; (c) 15% PCL with 0.1% silver; (d) 15% PCL with 0.5% silver; (e) 15% PCL with 1% silver. Scale bar 10 μm.

mean diameter increased to 495.2 nm and 540.6 nm respectively. Increasing the AgNP concentration to 1% did not further enhance the mean diameter (535.6 nm); however, it resulted in a small amount of fibers with a diameter over 1 μm.

The distribution of nanofibers within the scaffold was analyzed in three sections: top, middle and bottom regions. The data are summarized in Fig. 6b. It appears that a higher viscosity led to an overall

lower fiber density. The fiber density of 15% PCL was over 50% less than that of 10% PCL. A decrease in electrical conductivity resulted in a larger variation of fiber density across the three regions. For 15% PCL with 0.1% AgNP and 0.5% AgNP, more fibers were accumulated in the top region of the scaffold than in the bottom region because of the repulsive effects from the residual charges on the nanofibers. However, when the AgNP concentration increased to

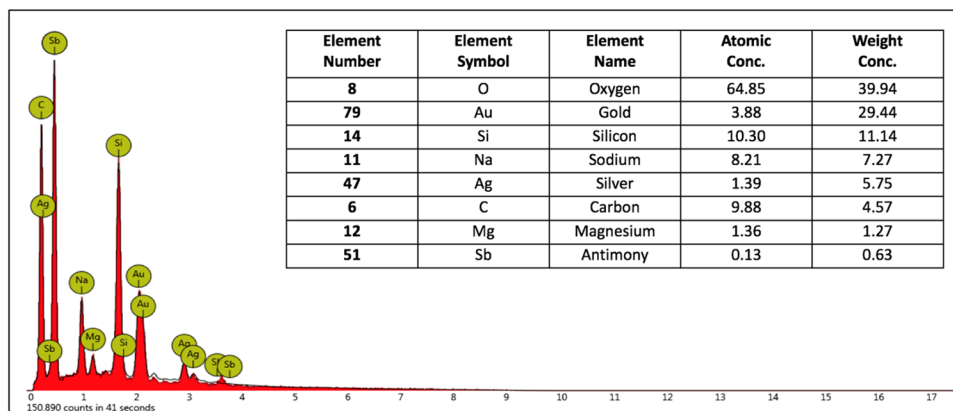


Fig. 5. EDS illustration for AgNP identification.

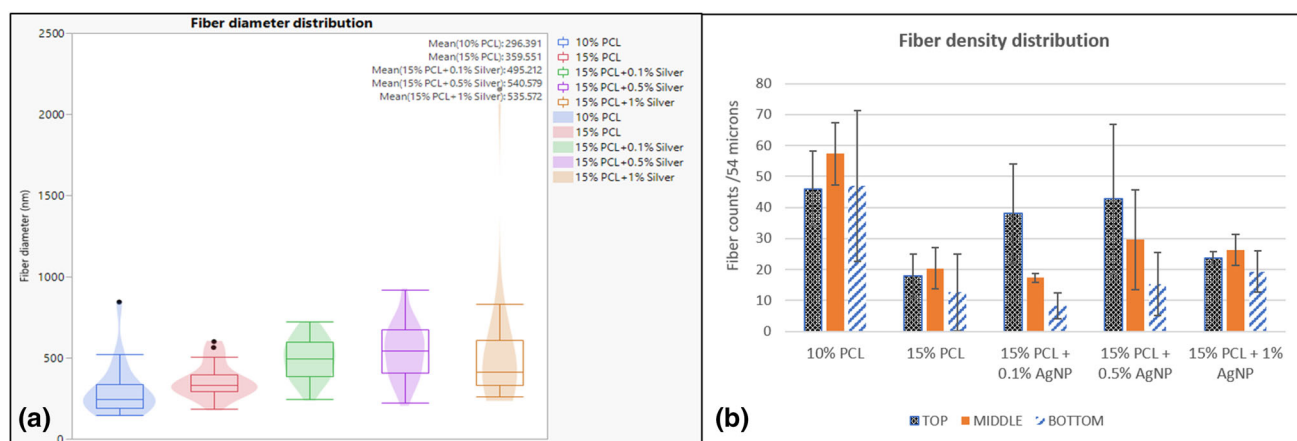


Fig. 6. (a) Nanofiber diameter distribution, and (b) nanofiber density distribution.

1%, the fiber distribution became more homogeneous. We speculate that this was due to a substantial increase in the mass of the nanofibers which compensated the electrostatic forces between them.

Representative images of cell culture are shown in Fig. 7. The cells stretched along the nanofibers after 24 h and proliferated within the scaffold in 7 days. The florescent image showed the cell skeleton and organization, proving that the nanofiber scaffold guided the cell alignment and growth.

DISCUSSION

In this study, we have presented a novel divergence electrospinning strategy to rapidly assemble aligned nanofibers along the z -axis by two axisymmetric and separately grounded bevels. This phenomenon was attributed to the whipping of the continuous electrospun jet in a symmetrically diverged electric field. While most of the nanofibers attached on either bevel of the collector, some remained between the two bevels due to the dragging effect of the whipping if the molecular cohesion of the liquid is sufficiently high to prevent stream breakup. We confirmed the hypothesis that, with a

given collector configuration, the formation of a 3D nanofiber structure was influenced by the viscosity of polymer solution. Gupta et al. found that, due to insufficient chain overlap in the 2D electrospinning process, only polymer droplets were formed in the dilute concentration regime.²² Our study shows that the threshold viscosity level for generating a 3D nanofiber structure is higher than that of a 2D nanofiber mat. One of the possible causes is that higher viscosity leads to higher surface tension, elasticity and plasticity, which provide increased resistance against the electrostatic force to sustain the elongation of polymer chains.²³ The high resistance also sustained the whipping effect of the continuous electrospun fiber jets in the symmetrically diverged electric field. If the plasticity is low, nanofibers will break into shorter pieces that attach only on the bevel surfaces without forming the bridging fibers inbetween.

The nanofibers were uniaxially aligned in the 3D scaffold. The results from fiber density analysis revealed a gradient of fiber density from the top to the bottom layers, and a decrease of fiber density from the top to the bottom, as well as from the periphery to the center. We hypothesized that this

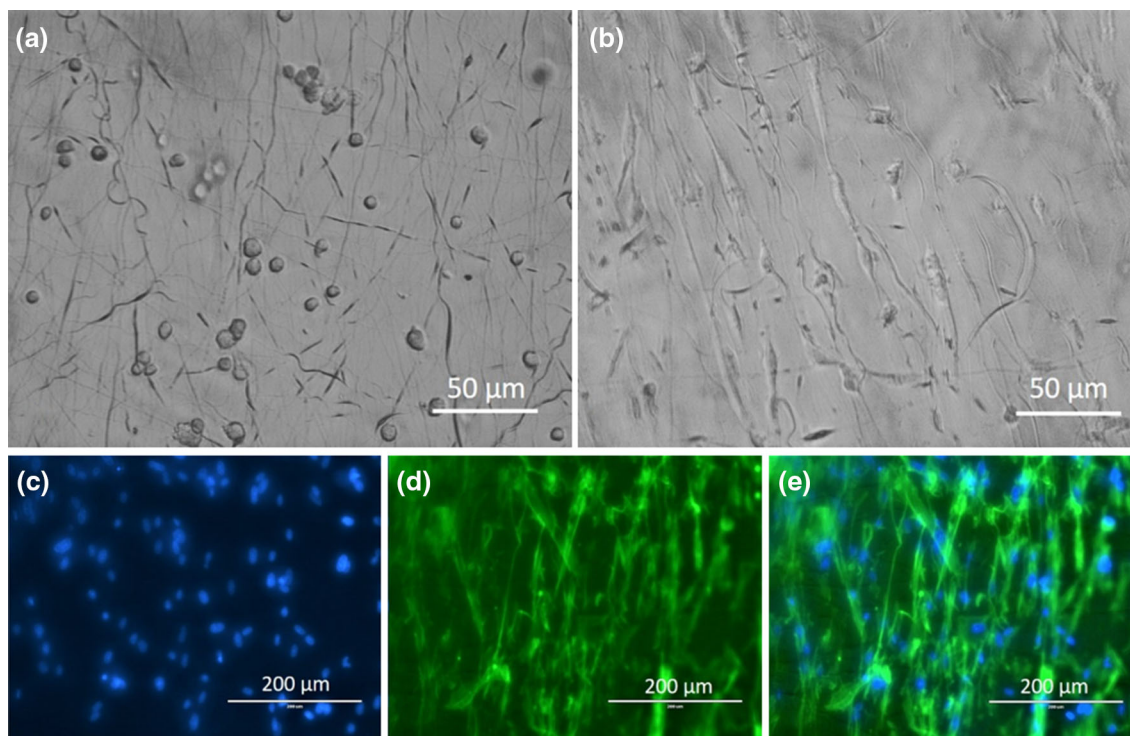


Fig. 7. Fibroblast cells seeded on the scaffold after (a) 2 h and (b) 24 h. Florescent cells after 7 days: (c) nucleus stained by DAPI, (d) cytoplasm by Phalloidin, and (e) an overlap.

phenomenon was due to the repulsive effects attributed to the residual charges on the electrospun nanofibers. For conventional 2D electrospinning, the nanofibers are deposited on a grounded surface, where the repulsive forces from the accumulated residual charges are fractional compared to the electrostatic force, until the fiber density and thickness reach a very high level. In our case, the bridging nanofibers were hanging between two grounded bevels. The electrostatic forces exerted on the nanofiber were diverged to two directions, leading to a weaker resultant downward force. When the nanofibers accumulated, the repulsive forces between the fibers might soon exceed the static electric forces and thus push the later electrospun fibers to the peripheral space. This results in a fast assembly of nanofibers along the z -axis. Once the nanofibers at the peripheral areas became denser, it would be more difficult for the electrospun jet to reach the central area. Therefore, the gradient of fiber density would only increase as the electrospinning continued.

According to our experimental results, a PCL solution with AgNP up to 0.5% led to a less homogeneous nanofiber distribution in the 3D space because of a lower conductivity. Smaller residue charges could be dissipated before new fibers were deposited, and therefore the electrostatic repulsion between the fibers increased. This resulted in a polarized fiber distribution with more fibers on top and fewer fibers at the bottom. On the other hand,

when the AgNP concentration increased to 1%, the weight of the electrospun fibers exceeded the upward electrostatic repulsion and thus more fibers accumulated in the bottom region which led to a more homogenous fiber distribution. This phenomenon indicated that the fiber density gradient can be reduced by either dissipating the residue charges through enhancing the electrical conductivity of the fibers or increasing the fiber density so that a larger gravity can overcome the electrostatic repulsion.

Recent studies have shown that the conductivity of the polymer solution also has effects on scaffold morphology. For example, Balogh et al. added non-surface-active salts of sodium dodecyl sulfate in hydroxypropylmethylcellulose acetate succinate-polyethylene glycol solution for a several-fold increase in conductivity, and obtained excellent quality electrospun fibers with a desirable density.²⁴ Similarly, Katsogiannis et al. found that increased solution conductivity results in the elimination of electrospun beads and the formation of a porous surface; the fiber diameter also decreased in a certain range with increased conductivity.²⁵ An enhanced electric property may be desirable for special tissue engineering applications such as nerve and heart tissue regeneration.²⁶ In addition, AgNPs as an antimicrobial agent^{27–30} can be incorporated into electrospun nanofibers to enhance the antibacterial activity for biomedical applications.^{31,32}

In our cell culture test, cells were attached to the microfibers and grew along the fibers. This result is consistent with many previous studies on aligned fiber scaffolds. It has been reported that aligned micro- and nanofibers are favorable for replicating the ECM for specific tissues which are composed of perpendicularly interwoven collagen strips. An aligned electrospun fibrous scaffold can provide contact guidance for migration and extension, resulting in an elongation and alignment of the cytoskeleton and nuclei along the axes of the fibers.¹¹ The effect of contact guidance of aligned electrospun fibers on cell morphological changes was evident in other many cell types.^{33,34} The scaffold developed in this study can be directly embedded in cell-laden hydrogel. This technique can be applied in the engineering of musculoskeletal soft tissues such as tendons, ligaments, knee menisci, etc.,³⁵ where fibrous cytoskeletal organization is critical for tissue formation and functions.

CONCLUSION

This study has investigated the effects of solution viscosity and electrical conductivity on nanofiber attributes for the divergence electrospinning technique based on the PCL solution. The addition of AgNPs into the PCL solution with organic solvents decreased the electrical conductivity. Our results showed that, at room temperature, the formation of a 3D nanofiber structure was determined by the solution viscosity. The minimum viscosity level was between 125 mPa s and 208 mPa s. The fiber density gradient was negatively correlated to electrical conductivity as well as fiber weight. The homogeneity in fiber distribution can be enhanced by increasing the electrical conductivity or the material density.

REFERENCES

- M. Santoro, S.R. Shah, J.L. Walker, and A.G. Mikos, *Adv. Drug Deliv. Rev.* 107, 206 (2016).
- C.J. Connon, *Procedia Eng.* 110, 15 (2015).
- B.M. Holzapfel, F. Wagner, L. Thibaudeau, J.-P. Levesque, and D.M. Huttmacher, *Stem Cells* 33, 1696 (2015).
- A. Skardal, M. Devarasetty, H.-W. Kang, I. Mead, C. Bishop, T. Shupe, S.J. Lee, J. Jackson, J. Yoo, S. Soker, and A. Atala, *Acta Biomater.* 25, 24 (2015).
- P.M. Mendes, *Chem. Soc. Rev.* 42, 9207 (2013).
- B.M. Baker and C.S. Chen, *J. Cell Sci.* 125, 3015 (2012).
- H.P. Shih, D. Panlasigui, V. Cirulli, and M. Sander, *Cell Rep.* 14, 169 (2016).
- C.S. Chen, *J. Cell Sci.* 121, 3285 (2008).
- Y. Zhou and G.Z. Tan, *Nanomater. Nanotechnol.* 7, 1847980417748478 (2017).
- A. Greiner and J.H. Wendorff, *Angew. Chem. Int. Ed.* 46, 5670 (2007).
- X. Wang, B. Ding, and B. Li, *Mater. Today* 16, 229 (2013).
- F. Du, H. Wang, W. Zhao, D. Li, D. Kong, J. Yang, and Y.Y. Zhang, *Biomaterials* 33, 762 (2012).
- M. Ramalingam, M.F. Young, V. Thomas, L. Sun, L.C. Chow, C.K. Tison, K. Chatterjee, W.C. Miles, and C.G. Simon Jr, *J. Biomater. Appl.* 27, 695 (2013).
- Y.J. Son, W.J. Kim, and H.S. Yoo, *Arch. Pharm. Res.* 37, 69 (2014).
- S.B. Orr, A. Chainani, K.J. Hippensteel, A. Kishan, C.L. Gilchrist, N.W. Garrigues, D.S. Ruch, F. Guilak, and D.W. Little, *Acta Biomater.* 24, 117 (2015).
- D. Kai, M.P. Prabhakaran, B. Stahl, M. Eblenkamp, E. Wintermantek, and S. Ramakrishna, *Nanotechnology* 23, 095705 (2012).
- M. Deng, S.G. Kumbar, L.S. Nair, A.L. Weikel, H.R. Allcock, and C.T. Laurencin, *Adv. Funct. Mater.* 21, 2641 (2011).
- B. Wulkersdorfer, K.K. Kao, V.G. Agopian, A. Ahn, J.C. Dunn, B.M. Wu, and M. Stelzner, *Int. J. Polym. Sci.* (2010). <https://doi.org/10.1155/2010/436178>.
- B. Ostrowska, J. Jaroszewicz, E. Zaczynska, W. Tomaszewski, W. Swieszkowski, and K.J. Kurzydowski, *Bull. Pol. Acad. Sci. Tech. Sci.* 62, 551 (2014).
- Y. Zhou and G.Z. Tan, Generation of 3D nanofiber structure by divergence electrospinning for tissue engineering scaffold, in *ASME 2018 13th International Manufacturing Science and Engineering Conference*. 2018. American Society of Mechanical Engineers, Paper No. MSEC2018-6543.
- B.E. Mbondo Tsamba, S. Sarraute, M. Traikia, and P. Hussion, *J. Chem. Eng. Data* 59, 1747 (2014).
- P. Gupta, C. Elkins, T.E. Long, and G.L. Wilkes, *Polymer* 46, 4799 (2005).
- S. Huan, G.X. Liu, G.G. Han, W.L. Cheng, Z.Y. Fu, Q.L. Wu, and Q.W. Wang, *Materials* 8, 2718 (2015).
- A. Balogh, B. Farkas, A. Pálvölgyi, A. Domokos, B. Démuth, G. Marosi, and Z.K. Nagy, *J. Pharm. Sci.* 106, 1634 (2017).
- K.A.G. Katsogiannis, G.T. Vladisavljević, and S. Georghiadou, *Eur. Polym. J.* 69, 284 (2015).
- D. Kai, M.J. Tan, M.P. Prabhakaran, B.Q.Y. Chan, S.S. Liow, S. Ramakrishna, and X.J. Loh, *Colloids Surf. B* 148, 557 (2016).
- S. Maharubin, Y. Zhou, and G.Z. Tan, *IEEE Trans. Nanotechnol.* 17, 948 (2018).
- Y. Zhou, S. Maharubin, P. Tran, T. Reid, and G.Z. Tan, *Environ. Sci. Water Res. Technol.* 4, 1511 (2018).
- Z. Tan, E.A. Havell, P.E. Orndorff, and R.A. Shirwaiker, *BioMetals* 30, 113 (2017).
- Z. Tan, G.N. Xu, P.E. Orndorff, and R.A. Shirwaiker, *J. Med. Biol. Eng.* 36, 325 (2016).
- Y. Wang, P.F. Li, P. Xiang, J.T. Lu, J. Yuan, and J. Shen, *J. Mater. Chem. B* 4, 635 (2016).
- Y. Liu, C. Hou, T. Jiao, J. Song, X. Zhang, R. Xing, J. Zhou, L. Zhang, and Q. Peng, *Nanomaterials* 8, 35 (2018).
- S.Y. Chew, R. Mi, A. Hoke, and K.W. Leong, *Biomaterials* 29, 653 (2008).
- L. He, S. Kiao, D. Quan, K. Ma, C. Chan, S. Ramakrishna, and J. Lu, *Acta Biomater.* 6, 2960 (2010).
- T. Jiang, E.J. Carbone, K.W.-H. Lo, and C.T. Laurencin, *Prog. Polym. Sci.* 46, 1 (2015).